QUARTERLY JOURNAL OF THE ROYAL METEOROLOGICAL SOCIETY
Q. J. R. Meteorol. Soc. **136(s1)**: 159–173 (2010)
Published online 24 August 2009 in Wiley InterScience
(www.interscience.wiley.com) DOI: 10.1002/qj.473

Synoptic variability of the monsoon flux over West Africa prior to the onset

F. Couvreux,[a]* F. Guichard,[a] O. Bock,[b] B. Campistron,[c] J.-P. Lafore[a] and J.-L. Redelsperger[a]

[a]*CNRM-GAME, Météo-France and CNRS, Toulouse, France*
[b]*LATMOS, IPSL, Paris, France*
[c]*Laboratoire d'Aérologie, OMP, Toulouse, France*

ABSTRACT: This study investigates the synoptic variability of the monsoon flux during the establishment of the West African monsoon using observations and ECMWF analyses. It highlights variability at a 3–5-day time scale, characterized by successive northward excursions of the monsoon flux. Their characteristics and climatology prior to the monsoon onset are presented. These penetrations follow a maximum of intensity of the heat-low (extension and minimum of pressure) and are concomitant with an acceleration of the low-level meridional wind. Some penetrations are stationary whereas others propagate westward simultaneously with African easterly waves. Both types are investigated in more detail by case-studies. This enables us to distinguish the boundary-layer mechanisms involved in such penetrations. A similar conceptual model holds for both. It is argued that the heat-low dynamics is a major driver of these synoptic penetrations, pointing to the predominantly continental nature of this phenomenon. In turn, the heat-low can be partitioned by the penetrations. Horizontal advection is the main process that eventually accounts for these surges; nevertheless, turbulent mixing also plays a significant role by vertically redistributing moisture, and in more subtle ways by its contribution to the shaping of the low-level synoptic environment within which the surges take place. Copyright © 2009 Royal Meteorological Society

KEY WORDS West African monsoon; heat-low; moisture surge; pre-onset period

Received 2 December 2008; Revised 4 May 2009; Accepted 8 June 2009

1. Introduction

The West African monsoon (WAM) provides most of the rainfall over the Sahel. The establishment of the monsoon flux over West Africa has been explored by a few studies; in the following the monsoon flux is denoted as $\phi_q = \rho.v.q$, with ρ the air density, v the meridional wind and q the water vapour mixing ratio. Sultan and Janicot (2003) have identified a 'pre-onset' stage corresponding to the arrival of the intertropical discontinuity (ITD) at 15°N with a climatological date around 14 May (with a standard deviation of 9 days) and an 'onset' stage corresponding to an abrupt latitudinal shift of the intertropical convergence zone (ITCZ) from 5°N to 10°N with a climatological date around 24 June (with a standard deviation of 8 days). Several hypotheses have been proposed to account for the abruptness of the onset of the WAM, emphasizing the role of the ocean (Eltahir and Gong, 1996), or the role of the atmosphere dynamics or both; Sultan and Janicot (2003) propose that the intensification of the heat-low increases the cyclonic circulation leading to a larger influx of moisture from the ocean. They also indicate a possible role of orography that could enhance the low-level circulation by favouring a leeward trough. Ramel *et al.* (2006) also emphasize the role of the heat-low but through thermal forcing linked to surface albedo instead of a more dynamical forcing. Hagos and Cook (2007) show, using regional climate budget analysis, the important role of the boundary-layer circulation and supply of moisture in preconditioning the atmosphere. All these studies have focused on relatively large time-scales (>10 days) and spatial scales (>2°) and have systematically removed the higher-frequency signals from the different fields in their analyses. In this study, we investigate the higher-frequency fluctuations of the water vapour as revealed by observations and operational analyses during the period preceding the 'onset', corresponding to the phase of establishment of the monsoon flux.

The WAM is a complex system presenting many interacting processes (see fig. 1 of Redelsperger *et al.* (2002) and Peyrillé *et al.* (2007)). One of the elements of the WAM that has not been highlighted much in the literature is the monsoon flux. In particular, it plays a central role in the water vapour budget over the area. In West Africa, the water vapour variability eventually results from strongly interacting phenomena such as moist convection, wave activity, dry intrusions and monsoon flux. Here, we focus on the variability in the low levels of the atmosphere and at synoptic time-scale and therefore investigate the variability of water vapour due to the monsoon flux.

Only a few studies have focused on the variability of the water vapour and of the monsoon flux over

*Correspondence to: F. Couvreux, CNRM-GAME, Météo-France and CNRS, 42 avenue G. Coriolis, 31057 Toulouse, France.
E-mail: fleur.couvreux@meteo.fr

West Africa. Cadet and Houston (1984) analysed the precipitable water for the summer of 1979 using European Centre for Medium-Range Weather Forecasts (ECMWF) analyses and integrated water vapour (IWV) derived from TIROS satellite data. They found that the main periodicities of IWV lie in the range 3–4 days and 6–9 days. Cadet and Nnoli (1987) investigated the water vapour flux variability using the same data. They showed that low-level flux (below 850 hPa) at 12°N was mainly southerly with variability at 3.5 days and 5–6 days. Here, continuing this work, we aim at understanding the key features of the successive northward penetrations of the West African monsoon flux prior to the onset. By analysing the phase preceding the 'onset', deep convection has only a limited impact on this variability in the Sahel region. This period has not been studied much even though it is the phase of establishment of the monsoon flux.

Two key elements of the WAM play a significant role in the mechanisms highlighted in this study: the Saharan heat-low (SHL) and the African Easterly Waves (AEWs). The SHL is a shallow disturbance, generally confined below 700 hPa (Lavaysse *et al.*, 2009). This SHL is characterized by an oscillation of about 5 days as revealed by Bounoua and Krishnamurti (1991). Parker *et al.* (2005), using 9-day high-pass filtered temperature and wind, suggest that on time-scales of a few days the intensity of the SHL influences the intensity of the monsoon circulation further south, and therefore affects the West African moisture budget. Peyrillé and Lafore (2007) have also emphasized the role of the SHL in controlling the northward penetration of the monsoon. Smith (1986) studies the radiative budget of the Arabian heat low. He relates the existence of moisture perturbations to an intensification of the heat-low, forcing a moisture inflow. He proposes two possible mechanisms for this intensification: a direct mechanism where an intensification of the surface heating leads to an increase of the pressure gradient and then to an advection of moisture, and an indirect mechanism resulting from a convectively induced subsidence warming.

The African easterly waves (AEWs) are westward-propagating synoptic disturbances characterized by a wavelength of 2500/3000 km and 3–5 days period (Reed *et al.*, 1977). They grow on both sides of the African Easterly Jet (AEJ) and are most active in August–September. They strongly modulate rainfall, convection and monsoon flux (Diedhiou *et al.*, 1999; Mekonnen *et al.*, 2006). To the north of the AEJ, convection remains in the southerly flow throughout the wave's trajectory (Duvel, 1990; Kiladis *et al.*, 2006). There is still no consensus regarding the source region of AEWs and the mechanisms for their genesis. Equatorial waves also play a role in West Africa (Wheeler and Kiladis, 1999; Mounier *et al.*, 2007) for time-scales of 6 to 7 days. Nevertheless, as shown by the latter study, they affect the easterly flow and are not really a modulation of the monsoon flux.

The main objective of the present paper is threefold: (1) to show the existence of monsoon flux penetrations at synoptic scale, (2) to identify their characteristics, and (3) to propose mechanisms accounting for such a mode of variability. We will also look at the interactions with AEWs that display similar time-scales of variability. This study is based on observations acquired during special observing periods (SOPs) of the African Monsoon Multidisciplinary Analysis (AMMA) programme (Redelsperger *et al.*, 2006) and on ECMWF operational analyses for four years, available every six hours at 0.25° (0.35°) horizontal resolution for 2006 and 2007 (2004 and 2005), respectively. Even though the diurnal cycle is an important mode of variability of the WAM (Parker *et al.*, 2005; Lothon *et al.*, 2008), it is not directly addressed in this paper. The remainder of this paper is organized as follows: section 2 presents the synoptic variability of the water vapour as inferred from observations and analyses, highlights the existence of successive moisture northward penetrations and describes their mean characteristics. Two types of penetrations are identified, stationary and propagative ones. Section 3 presents two case-studies illustrative of each type of penetration. In this section, mechanisms involved in the penetration are discussed. Section 4 indicates the proposed criteria to define such events and discusses the other factors modulating these features. The paper concludes with a summary in section 5.

2. Evidence of moisture penetrations

2.1. From observations

According to Janicot *et al.* (2008) the dynamical monsoon onset occurred in 2006 around 25 June whereas the increase of rainfall over the Sahel really started around 10 July (with a 15-day delay). In the period ranging from the pre-onset to the onset, fluctuations in the Integrated Water Vapour (IWV) derived from six Global Positioning System (GPS) stations (located in Figure 1), installed over West Africa during AMMA (see Bock *et al.* (2008) for the description of this GPS network), are evident as shown in Figure 2(a). The variations are larger in intensity in the northern stations (standard deviation of 6 kg m^{-2}, representing more than 20% of the mean value, about 30 kg m^{-2}) than the southern stations (standard deviation of 3 kg m^{-2}, representing only 7% of the mean value, about 45 kg m^{-2}). Note that there is no trend in the IWV during the period (referred to as period B in Bock *et al.* (2008), see also their fig. 10) from the pre-onset to the onset (Figure 2(a)). This variability is not specific to 2006 and is also present in GPS observations for the same period of 2005 and 2007 and in ECMWF analyses for 2004, 2005 and 2007 (see below). These fluctuations are characterized by a time-scale larger than 24 hours but smaller than 10 days. This is in line with the wavelet decomposition of the IWV at the northernmost stations (Tombouctou and Gao, ∼16°N) illustrated for the Gao station in Figure 2(b), which indicates a strong signal at 3–6 days, consistent with Cadet and Nnoli (1987). Decomposition for Sahelian stations (Niamey and Ouagadougou, ∼13°N) emphasizes a peak at slightly shorter periods, about 1.8–4 days. Finally, at the Guinean

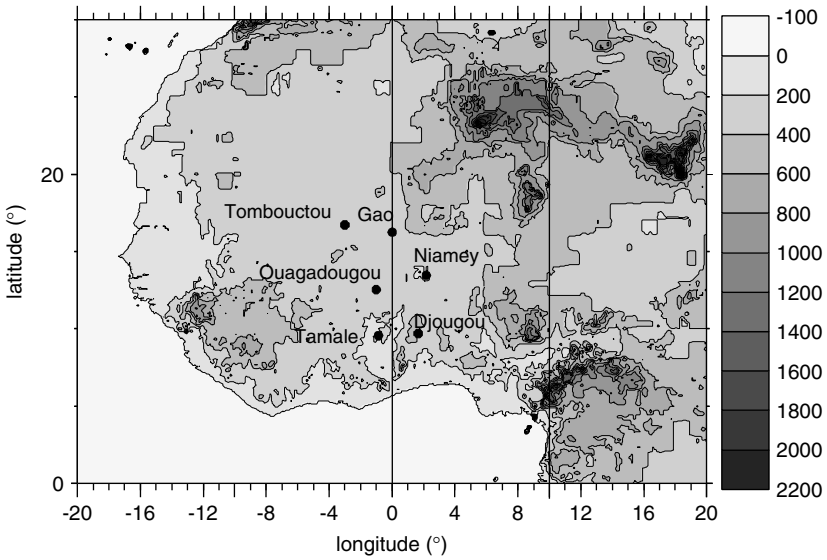

Figure 1. Domain of the study: West Africa and its topography (contours every 200 m). The six GPS stations are localized by black dots. Vertical lines also specify the area used for the zonal mean.

stations (Tamale and Djougou, ∼9.5°N) IWV displays various peaks with a larger diurnal signal and other periods of 3–5 days (see Bock *et al.* (2008), their fig. 11). The maximum amplitude of these fluctuations occurred in the period preceding the monsoon onset and also, to a lesser extent, during the monsoon retreat (in September) especially for the northernmost stations (see an illustration in fig. 10 of Janicot *et al.* (2008)). Note that there is also some variability at larger time-scale in the 10–20-day range at the different locations; this is however not the focus of this paper.

Data from radiosondes launched four times a day at Niamey also reveal such variability. Note that for this study, only the Vaisala-92 type of sonde has been used, which is not expected to be affected by large humidity biases (Nuret *et al.*, 2008). As shown in Figure 3, the fluctuations of IWV are mainly due to the contribution of the low levels, up to 3 km above ground level (this height was selected as corresponding to a mean afternoon boundary-layer height averaged over the period). Low levels of the atmosphere, i.e. below 3 km (respectively 2 km) contribute to more than 75% (58%) of the IWV and 88% (respectively 72%) of its variability. At 5000 m, almost the entire IWV is already gathered by the levels below suggesting a very weak role for upper-level moisture in the variability of IWV during this period. The AEJ core layer (about 4 km) also contributes little to this variability. The large contribution of the low levels to the IWV variability (Figure 3(b)) reflects the impact of the monsoon flux variability (Figure 3(c)); the correlation is 0.67. Larger monsoon flux is due to the deepening of the monsoon layer, and to the intensification of both the meridional wind and the water vapour content in that layer, the three components contributing equally (Figure 3(c)).

In short, AMMA observations show a large variability of the IWV at time-scales from 3 to 6 days, which is mainly due to variability of the monsoon flux intensity and depth.

2.2. From ECMWF analyses

Taylor *et al.* (2005) and Thorncroft *et al.* (2003) have indicated that ECMWF analyses provide valuable information on the low-level thermodynamic patterns. Flamant *et al.* (2007, 2009) showed a good agreement of ECMWF analyses for 5 and 6 June 2006 with observations particularly for the position of the ITD and the thermodynamic profiles. This study uses mainly the 2006 ECMWF analyses that benefited from a higher resolution, 0.25° (against 0.35° for the previous years), and a larger amount of data (radiosondes, surface meteorological stations) assimilated during the AMMA SOP. Nevertheless, as GPS data are not assimilated, they provide an independent source of information from the previous section. In complement, 2004, 2005 and 2007 ECMWF analyses were also used to check the generality of our findings. Some changes in the assimilated data and the physics of the model occurred during these years; nevertheless the characteristics deduced from these analyses are consistent throughout these years. Moreover, IWV from ECMWF analyses has been evaluated in 2005 and 2006 and shows good agreement with GPS data at the synoptic scale (Bock *et al.*, 2008).

ECMWF analyses also exhibit similar moisture fluctuations as revealed by GPS. In Figure 4, about 11 quasi-periodic northward excursions of high IWV (over 35 kg m^{-2}) take place north of 14°N from 15 May to 30 June 2006. Figure 4 shows fields averaged over [0–10°E] (the results are not sensitive to the choice of window longitude used for averaging, [5°W–5°E] or [10°W–10°E] give similar results). The moisture penetration has a longitudinal extent varying from 500 to 1000 km. These moisture increases follow a minimum in mean sea-level pressure (MSLP, below 1006 hPa at 1800 UTC) at about 16°N and are slightly ahead of an increase of the meridional 925 hPa wind revealing an intensification of the monsoon flux. The ITD also records these fluctuations in

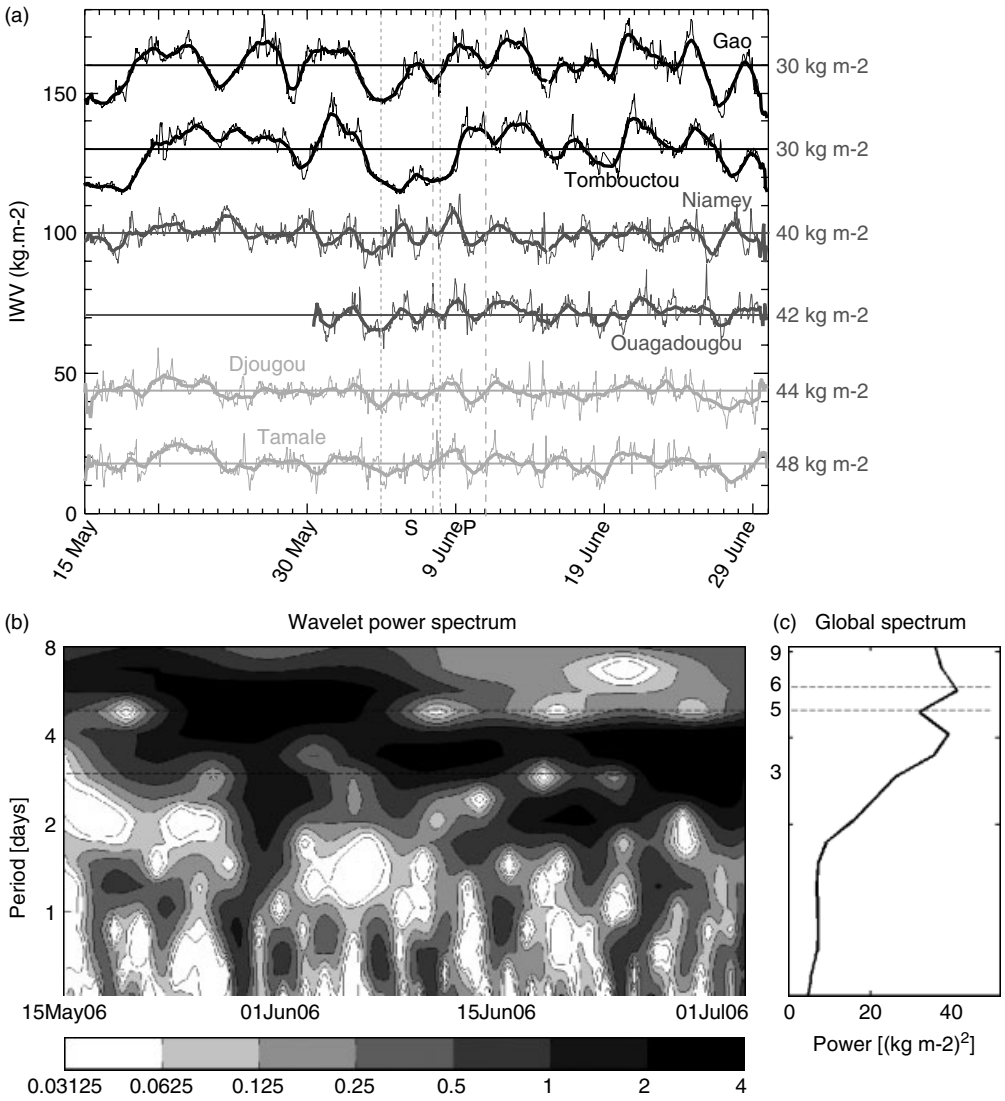

Figure 2. (a) Integrated water vapour (IWV) measured at six GPS stations in the AMMA area from 15 May to 30 June 2006. The thick lines correspond to the IWV filtered to remove diurnal variability. The black lines correspond to northernmost stations (Gao and Tombouctou), the dark-grey lines to Sahelian stations (Niamey and Ouagadougou) and the light-grey lines to Guinean stations (Djougou and Tamale); see Figure 1 for their locations. To avoid superposition a constant value is added with respective values of 130, 100, 60, 30, 0, −30 kg m^{-2}. The mean value over the period is indicated on the right side. (b) Wavelet spectrum as a function of time and (c) the mean spectrum of the unfiltered IWV for Gao station.

agreement with Bock *et al.* (2008) who show that the ITD is well correlated to the 30 kg m^{-2} contour (Figure 4, white contour). Inspection of ECMWF analyses for other years (pre-onset periods of 2004, 2005 and 2007) reveals that such IWV variations are common features over the area and well resolved by the ECMWF analyses.[†] In the following, we will call this northward moisture excursion 'moisture surge'. Horizontal map inspection indicates that among the 11 northward excursions for 2006, some are propagative: in fact, five are stationary and six propagate westward (see Hovmüller diagram of IWV in Figure 5). Surges are considered propagative if there is concomitantly a westward propagation for at least 1000 km (the average size of a surge) and a phase velocity of 6–10 m s^{-1} of the meridional wind at 850 hPa and the IWV. For the same period, there were 11 surges in 2004, 9 in 2005 and 9 in 2007, among them 7 (4) stationary (propagative, respectively, the others being undetermined, see section 2.4) in 2004, 3 (4) in 2005 and 3 (5) in 2007. So, 2006 is representative of other years.

Surges are present from April to October. From April to mid-May (respesctively, in October) the moistening (drying) trend corresponding to the arrival (retreat) of the monsoon dominates (fig. 10 of Janicot *et al.*, 2008). During the core monsoon season (July and August), surges are less periodic, more abrupt and with larger latitudinal extensions; such features may be related to the more widespread occurrence of moist precipitating convection then, a process that complicates the mechanisms (see an example in Barthe *et al.* (2009)).

[†]NCEP2 reanalyses also indicate such surges.

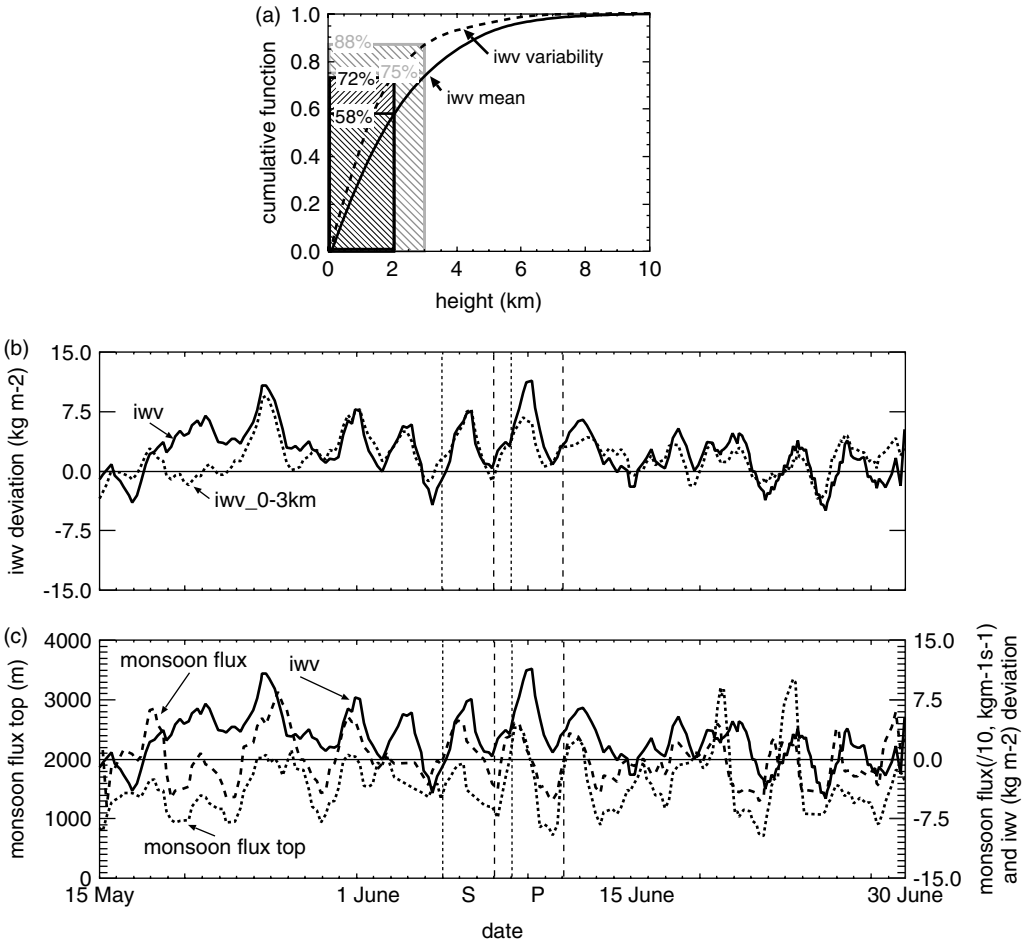

Figure 3. (a) Cumulative function as a function of height of the integrated water vapour mean and standard deviation: the black (grey) boxes indicate the contribution of the levels below 2000 m (3000 m) to the IWV mean and standard deviation. (b) Time series of IWV deviation (deviations are computed relatively to the period mean) and low-level (up to 3 km) contribution from Niamey radiosondes launched four times a day (but with the diurnal cycle filtered out, also deviations from the period mean of the contribution) from 15 May to 30 June 2006. (c) Top of Φq (defined as the first vertical level where the meridional wind changes from northward to southward), Φq intensity (i.e. the monsoon flux vertically integrated up to its top) and IWV deviation. Vertical dotted and dashed lines indicate the two case-studies.

2.3. Generic features of the water vapour surge

Surges (as defined above) last a day to a few days with a mean duration ($< T >$) slightly longer than two days. The characteristic period of the entire surge is about 4.5–5 days, in agreement with GPS observations. They occur regularly especially before the onset. A composite of the surge is presented here. It is derived from ECMWF analyses (for the pre-onset to the onset period, from 15 May to 30 June, for the four years) using an IWV criterion: a surge is present if there is a positive anomaly (over 1 kg m^{-2}) of the IWV averaged over [0–10°E, 14°N–20°N] relative to the 10-day mean. Only events lasting more than a day and separated by more than a day from the previous and following surge are selected for this analysis (about 60% of the surges, 24 cases in total, are selected due to these constraints). According to the composite, a surge is characterized by a relatively high pressure in the latitude range [14°N–20°N] compared to the preceding and following period with a mean difference of about 1.5 to 2 hPa (Figure 6). The beginning of a surge is characterized by an increase of the 925 hPa meridional winds up to 3 m s^{-1}. As expected, during a surge, a northward displacement of the Intertropical Discontinuity (ITD) is evident in thermodynamic criteria (e.g. IWV gradient or 15°C dew-point) and dynamic criteria (the latitude of zero zonal wind or meridional wind). Here the diagnostic based on the meridional wind can be used as it is computed from [0–10°E] averaged fields; this diagnostic highlights a lot of variability at smaller scales. The meridional wind criterion shows a much larger northward penetration than the moist criterion, suggesting that the large IWV is not advected up to the northward limit of the southerly wind.

In this figure, a strong link between the heat-low dynamics and the monsoon flux is implied by the acceleration of the northward flux after the minimum of pressure is reached. The pressure fluctuations have a period of 4.5 days in this composite in agreement with Bounoua and Krishnamurti (1991). An increase of the ventilation from the northeast by the Harmattan wind (north of 22°N) is also noticeable before the surge; it brings drier air (Figure 6) and might participate in the recovery phase. Its role needs further investigation and is beyond the scope of this paper. Moreover, ECMWF analyses indicate that the

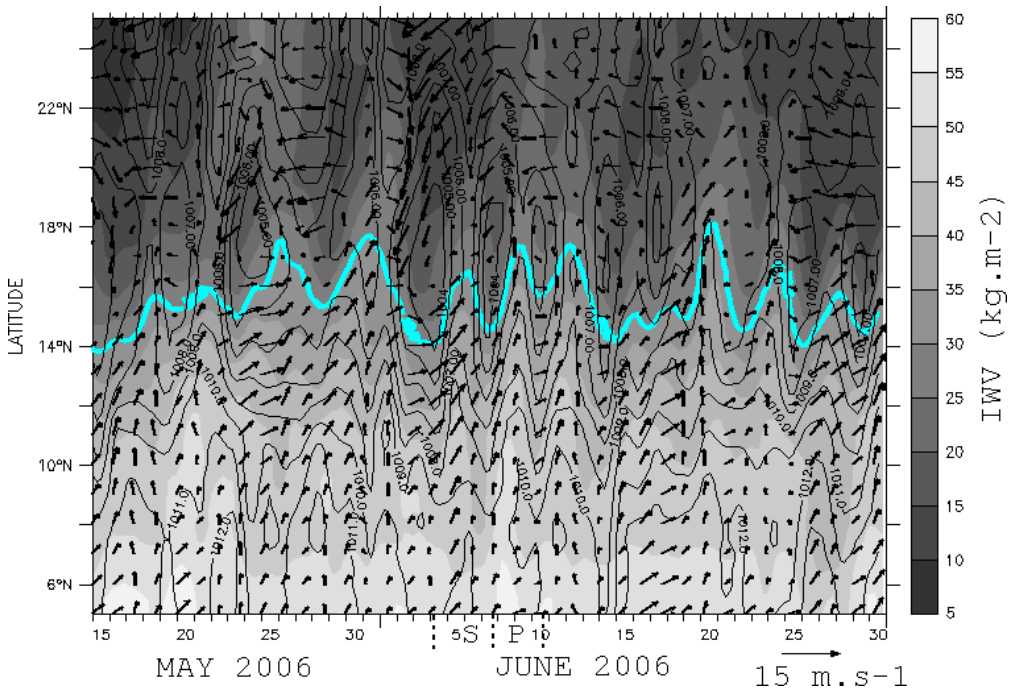

Figure 4. Time–latitude diagram of ECMWF analysis IWV (shaded in kg m^{-2}), MSLP at 1800 UTC (black isocontours in hPa) and 925 hPa wind (black arrows in m s^{-1}), averaged over [0–10°E] from 15 May to 30 June 2006. The dotted lines along the x-axis indicate the stationary and propagative case-studies. The white full line corresponds to the limit of IWV=30 kg m^{-2}. This figure is available in colour online at www.interscience.wiley.com/journal/qj

surge maximum is correlated with the strong low-level jet in the early morning at 0600 UTC (not shown). This is confirmed by the UHF (ultra-high frequency) radar wind profiler, operating continuously at Niamey Airport (see Kalapureddy *et al.* (2009) for more details) that provides measurements of the horizontal wind component for the two case-studies.

Interestingly, such surges occur in the zonally symmetric model of the West African monsoon (Peyrillé *et al.*, 2007) but with a weaker amplitude with concomitant maximum of surface temperature (increase of 0.5 K) and minimum of MSLP (decrease of −0.5 to −1 hPa versus −2 hPa in the ECMWF composite, cf. Figure 6) in the heat-low area followed by an increase of the northward component of the 10 m wind (0.5 m s^{-1} versus 2 m s^{-1}) and then an increase of the surface water vapour mixing ratio (0.5–0.7 g kg^{-1}). The occurrence of such surges in this model implies that their existence does not require the presence of an AEW, as they cannot be represented in this two-dimensional configuration.

2.4. Interactions with easterly waves

Figure 5 presents Hovmüller diagrams computed for the IWV (shading) and Tropical Rainfall Measurement Mission (TRMM) rain-rate estimates (isocontours) in (a) and (c) and for meridional wind at 700 hPa in (b) and (d) for two years, respectively 2006 (a) and (b) and 2004 (c) and (d). Hovmüller diagrams of meridional wind show the existence of AEW during the period from pre-onset to onset with high meridional wind perturbations propagating westward with a mean velocity of 8.5 m s^{-1}. The 700 hPa altitude, corresponding to the maximum of the zonal wind (observed between 700 and 600 hPa) has been chosen in order to separate the impact of the monsoon flux variability and oscillations of the jet. For this period, the AEJ is located at about 11°N. Note that similar results are obtained for 850 hPa, a more traditional altitude of detection of waves north of the jet according to Pytharoulis and Thorncroft (1999) and Janicot *et al.* (2008). Several surges propagate westward simultaneously with AEWs as is obvious on the IWV (Figure 5, 7 to 12 June 2006 for example). This is consistent with the frequent time-lag observed in GPS IWV fluctuations between Gao and Tombouctou (Figure 2; the correlation is maximum with a lag of half-a-day, corresponding to a propagation speed of about 7.5 m s^{-1} consistent with AEW speed). In the first part of the period, the wave occurrence is weak compared to the second part of the period when anomalies of IWV or meridional wind propagate westward (in agreement with diagnostics from Berry *et al.* (2007)). Figure 5 indicates the stationary and propagative surges for the two years. The moisture surges tend to occur simultaneously with the southerly sector of the AEW. On average, less than half of the surges (44%) are stationary whereas the other half (48%) propagate westward (8% are undetermined). The next section begins with an analysis of a stationary surge (corresponding to the case S of Figure 5) to avoid complexity from interactions with AEWs. A propagative surge (corresponding to the case P of Figure 5) is then studied to highlight the interactions with AEW. Figures 5 also show a complex relationship between rain-rates (estimates from TRMM: Huffman *et al.*, 2007) and the

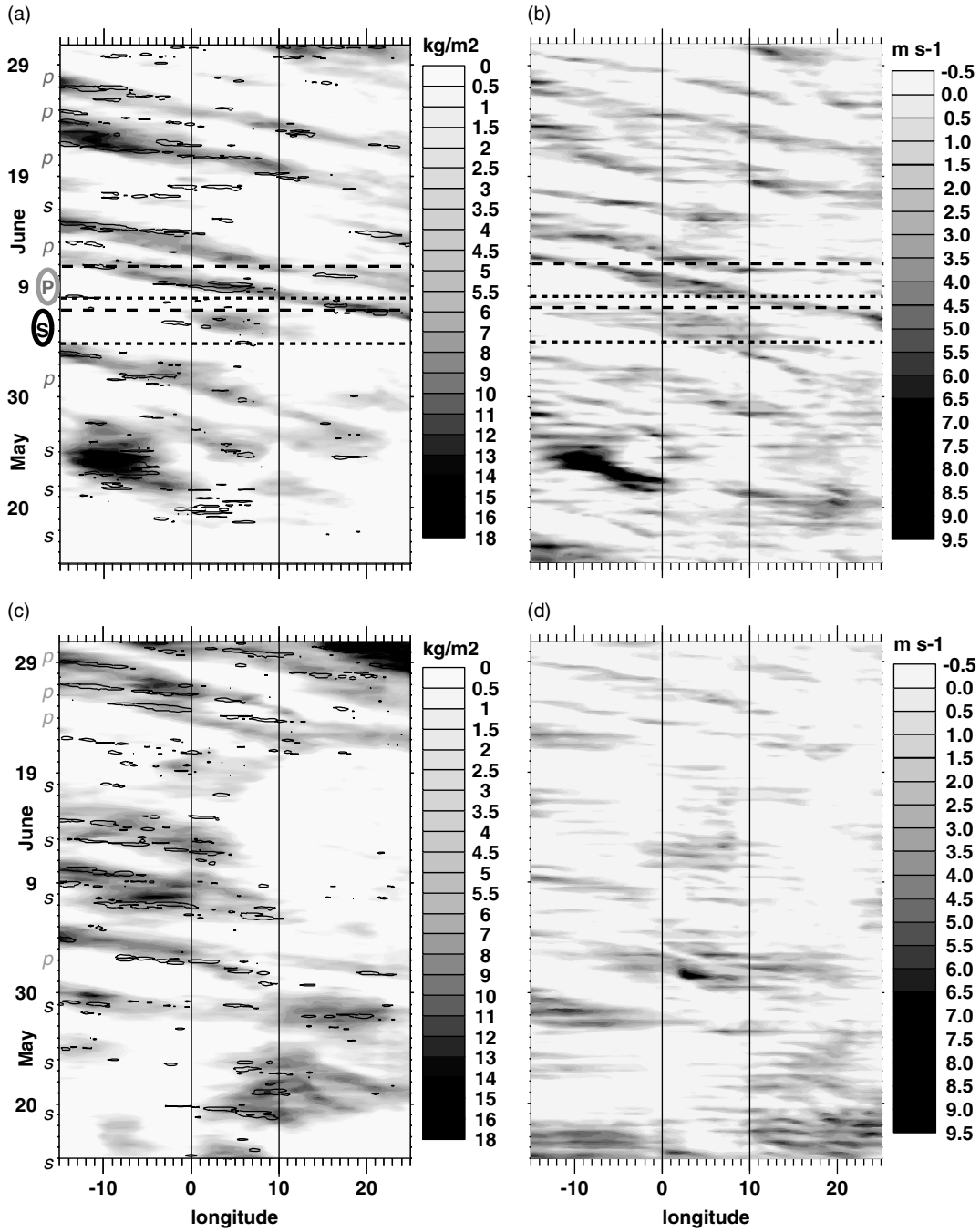

Figure 5. Hovmüller diagram of (a) and (c) TRMM (Tropical Rainfall Measurement Mission) rain-rate (isocontours every 0.25 mm/h, 3B42 product) and the IWV deviation from the zonal mean (shading, only positive anomalies are drawn for clarity) and (b) and (d) deviation from the zonal mean of the meridional wind at 700 hPa averaged over [13°N–20°N] from 15 May to 30 June 2006 (a) and (b) and 2004 (c) and (d). Stationary and propagative surges are indicated by an *s*, respectively *p*, in the left margin for the two years. S is the first case-study, where no AEW is present; P corresponds to the second case-study where AEW exists. The vertical lines define the zone of focus from 0°E to 10°E.

surges. During most of the surges rainfall is recorded, nevertheless precipitation also occurs without surges. This suggests that surges can favour deep convection but are not the only component.

3. Two case-studies: a propagative and a stationary surge

In this section two case-studies are presented in order to highlight the processes involved in the surges. Here, the investigation of the case-studies is based primarily on ECMWF analyses.

3.1. The 4–7 June 2006 case, a stationary surge

This case is detailed first as exhibiting a zonally non-propagating behaviour as shown in Figure 5. This period is characterized by low wave activity as indicated by the objective techniques of AEW detection (Berry *et al.*, 2007; Thorncroft *et al.*, 2007). It is expected to highlight

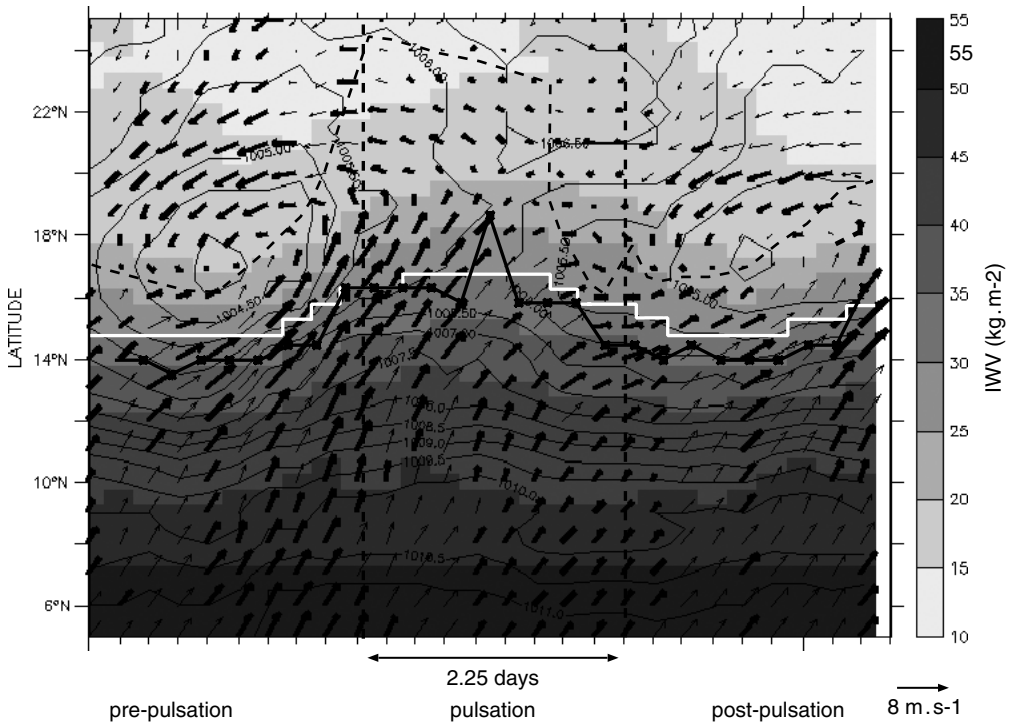

Figure 6. Composite moisture surge showing IWV (shaded in kg m^{-2}), MSLP with diurnal variability removed (black lines in hPa, isocontours separated by 0.5 hPa) and 925 hPa horizontal wind (black arrows) obtained for the pre-monsoon period (15 May to 30 June) for the years 2004 to 2007. All fields are averaged over [0–10°E]. The dashed lines delimit respectively the period before and after the surge. ITDs derived from the gradient of IWV (full black line) and from the zero 925 hPa meridional wind (dashed black line) are overplotted. The white line corresponds to the limit IWV=30 kg.m^{-2}. The bold vectors correspond to the winds significant at 95% according to Student's *t*-test.

key features without the complications arising from interactions with AEWs.

3.1.1. Synoptic conditions

From 3 to 7 June, there is a relatively strong subtropical jet at 200 hPa. An upper-level trough is present at this altitude moving slightly to the east. The African Easterly Jet lies at 11°N. A high-pressure system is located over the Mediterranean coast inducing strong north-easterly low-level winds north and west of the Hoggar (Flamant *et al.*, 2007). Early on the morning of 5 June, a mesoscale convective system is initiated north of Niamey; this is the only convective system presents during this 3–7 June period north of 12°N.

3.1.2. Surge description

In this section, we focus on both the spatial and temporal characteristics of the surge mainly based on ECMWF analyses. Figure 7(a) shows the time evolution from 3 to 6 June of horizontal maps of IWV, MSLP and 925 hPa wind at 0600 UTC. The northward surge of moisture lasts from 4 June to 7 June with a horizontal length of the moisture penetration of about 1000 km. The IWV positive anomaly remains centred around 5°E without any noticeable westward propagation from 4 to 5 June and the most northward penetration is located just south of the minimum of MSLP. It moves only slightly westward during 6 June. In fact, the advection of moist and cool air is associated with a cooling of the low levels; the thermal depression only persists on the border. The flow being on the right side of the thermal low due to the cyclonic circulation induces a spreading to the west. This is consistent with a mechanism proposed by Taylor *et al.* (2005) to explain westward shift of surface anomalies, but which involves interactions with deep convection and soil moisture. For this particular case, the spreading of a Mesoscale Convective System (MCS) cold pool (Flamant *et al.*, 2009) also participates to the north-westward shift of the IWV anomaly. The heat-low is stronger on 3 and 4 June at 1800 UTC with respective minima of MSLP of 1001 and 1002 hPa at the Niger–Mali border. Then, through the period, the intensity of the heat-low decreases. During this period, a striking feature is the splitting of the heat-low into two smaller cells: A larger cell expands from 5°W to 20°E from 3 to 5 June with a minimum of MSLP located at 5°E evolving into two small cells by 6 June 0600 UTC with two minima of MSLP at 13–15°E, 16°N and 8°W, 16°N. To our knowledge, this behaviour has not been mentioned previously but such splitting of the heat-low into different cells is found to be common. For this case-study at least, it is related to the penetration of the monsoon flow around 5°E that distorts and then breaks down the heat-low into two cells.

In Figure 8, the time evolution of selected variables derived from ECMWF analyses are indicated for this typical surge:

- The ITD (latitude of the 15°C dew-point at 925 hPa, shaded) reaches its most northern extension on

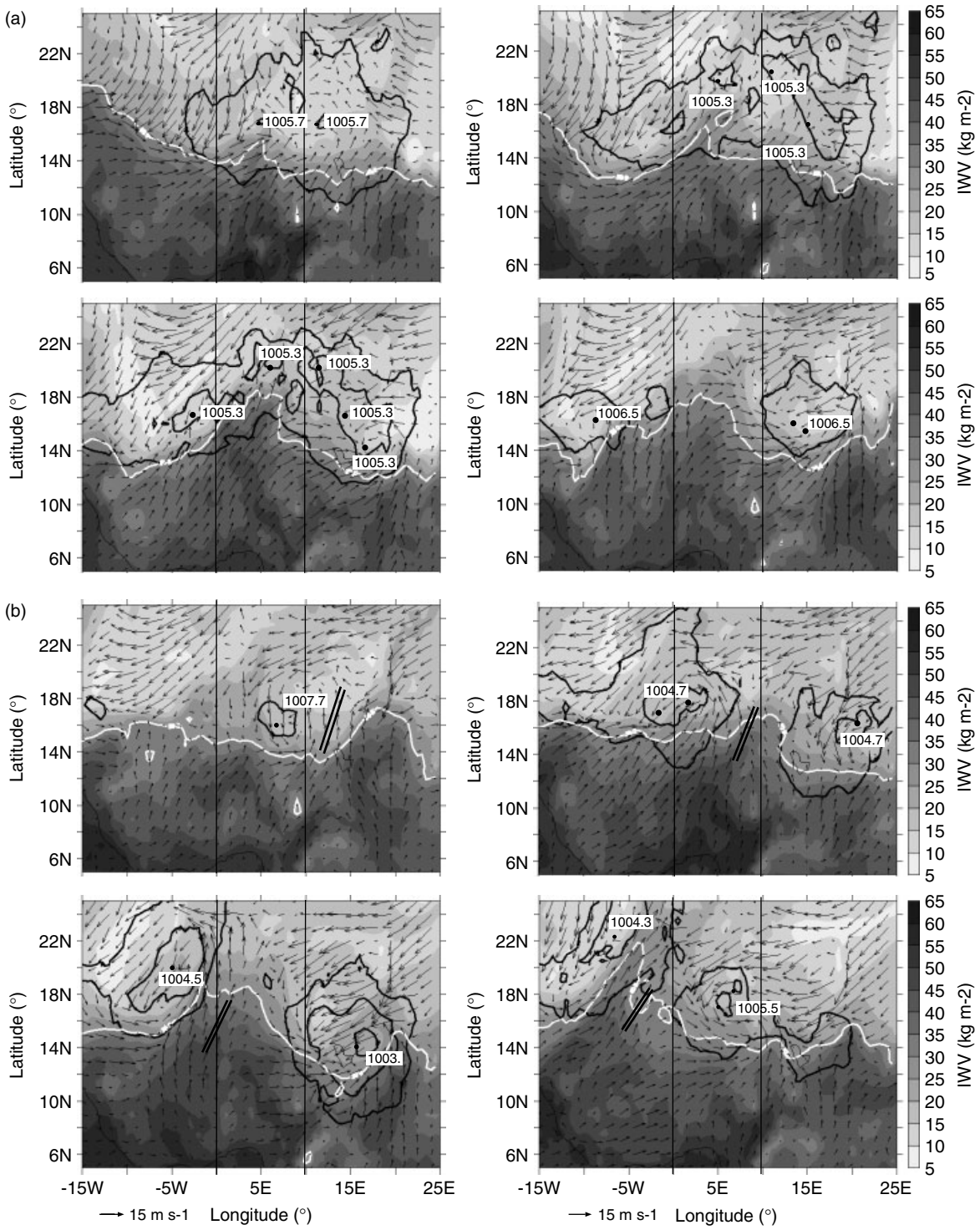

Figure 7. Horizontal maps of the IWV (shading), the MSLP (isocontours of 1006 and 1008 hPa are indicated), and the 925 hPa horizontal wind (vectors) at 0600 UTC. (a) From 3 to 6 June and (b) from 7 to 10 June from top left to bottom right. The white thick line corresponds to the contour of IWV=30 kg m^{-2}. The double black line indicates the position of the trough.

5 June. This is consistent with observations: the ITD, derived from surface station observations (from dew-point, not shown), shows a similar northward excursion reaching 18°N on 5 June 0600 UTC. The ITD exhibits a strong diurnal cycle that smoothes the signal of the surge, as shown in Figure 8(a). In the early morning, a northern extension and a sharper gradient of the water vapour mixing ratio are observed resulting from moisture advection from the low-level jet. In early afternoon, a southern localization and a smoother gradient result from a dilution of the moist area by turbulent mixing in the boundary layer during the day (Lothon *et al.*, 2008). Despite the strong diurnal cycle, the surges still induce large latitudinal modulations of the location of the ITD.

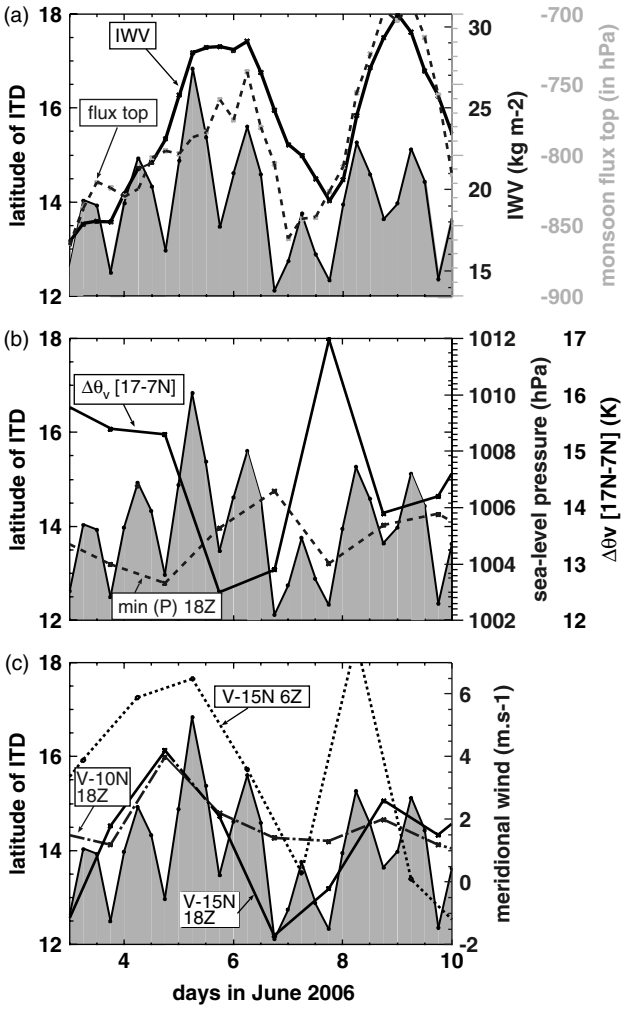

Figure 8. Time evolution for the two consecutive surges of variables averaged over [0–10°E]: The ITD latitude (derived from the 15°C dew-point at 925 hPa) is plotted on each graph by grey shading. In (a), the IWV averaged over [14–20°N, 0–10°E] and the monsoon depth (limit between southerly and northerly winds, this criterion is only used south of the ITD), in (b), the minimum of mean sea-level pressure (at 1800 UTC) over [14–20°N, 0–10°E] and the meridional virtual potential temperature difference between 17°N and 7°N at 1800 UTC and in (c), the 925 hPa meridional wind at 10°N and 15°N (at 0600 and 1800 UTC) are overplotted.

The maximum of IWV averaged over [14–20°N, 0–10°E] is reached at the same time and persists for an entire day. The maximum depth of the monsoon flux is registered on 6 June (Figure 8(a)). Soundings also reveal a deeper monsoon flux (reaching 2 km deep) on 5 June. The intensification of the monsoon flux is due to (1) the deepening of the monsoon flux, (2) its higher water vapour content (as indicated by the Niamey radiosoundings, not shown) and (3) the intensification of the meridional wind, in agreement with the general behaviour highlighted in Figure 3.

- On 3 and 4 June, the heat-low intensity increases (decrease of the MSLP, Figure 8(b)) with concomitant increase of the low-level temperature maximum (values are indicated at 1800 UTC). This leads to a larger pressure gradient, ΔP. Surface stations also record such variations with maximum of surface temperature and minimum of surface pressure (not shown). There is a lag between the heat-low maximum and the maximum of IWV.
- The low-level winds increase (Figure 8(c)) from 4 to 5 June with a maximum reached during the 4–5 June night. This is consistent with the Niamey sounding and UHF radar wind profiler data showing a wind speed of 15 m s^{-1} from 1800 UTC on 4 June to 1200 UTC on 5 June (Figure 9) over an increasing depth compared to the previous day (see Figure 3(b)). Note also that on both 4 and 5 June a strong low-level jet is indicated by UHF radar data (Figure 9). At the same time, no AEW trough is evident at the level of the AEJ during the whole period.

3.1.3. *Towards a conceptual model*

Based on this time evolution, we propose the following scenario for the surge. The high late-spring solar insolation acts to increase surface temperature. Through surface heat fluxes and dry convection, the boundary layer warms up leading to an increase of the heat-low intensity. This in turn leads to an intensification of the monsoon flux on the southeast flank of the heat-low (cyclonic circulation due to the low pressure) and an increase of southerly winds. Such enhanced monsoon flux favours a northward penetration of the ITD, an increase in the IWV north of 14°N and a deepening of the monsoon flux. This is confirmed by a maximum of ΔP followed by a maximum of meridional wind and then by a maximum of IWV (Figure 10). In this figure, the contribution of the heat low to the ΔP is indicated by the dot-dashed line, which represents the difference between the pressure over [14–18°N] and the monthly mean pressure at [8–12°N]. This indicates that the pressure variations north of 14°N primarily control the fluctuations of the ΔP (at this time-scale). This implies that the heat-low is the major driver of the surge.

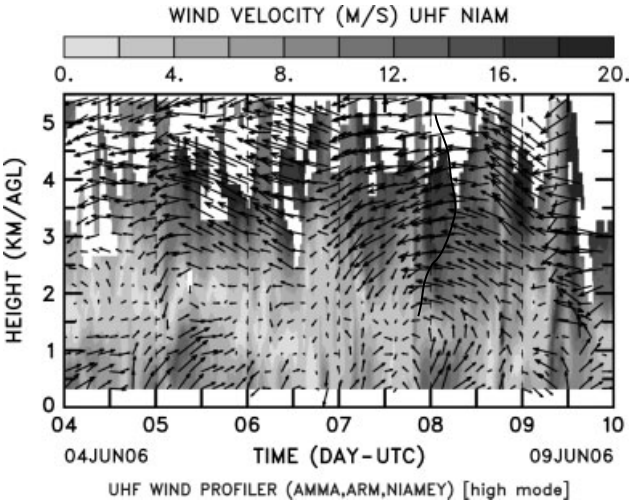

Figure 9. Vertical cross-section of horizontal wind (intensity in shading and direction in vectors) observed by the UHF radar located in Niamey from 4 to 10 June 2006. The black line indicates the position of the trough.

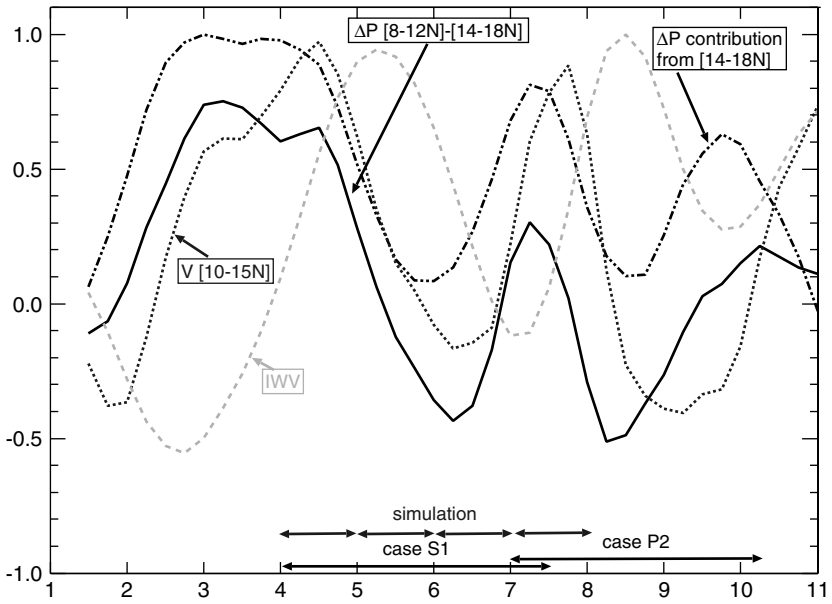

Figure 10. Time evolution from 1 to 10 June of one-day filtered, averaged over [0–10°E], IWV averaged over [14–20°N], meridional wind averaged over [10–15°N], MSLP gradient between [8–12°N] and [14–18°N] and the contribution of the heat-low to the pressure gradient (computed by the difference between the monthly mean of MSLP averaged over [8–12°N] and MSLP averaged over [14–18°N]. These fields have been normalised by the maximum and minimum values for June.

As the monsoon flux advects cooler and moister air, the heat-low strength overall weakens. This is confirmed by inspection of the temperature fields indicating a cooling at 925 and 850 hPa on 5 June and also the distortion and breakdown of the heat-low cell in Figure 7. Therefore the initial source of intensification of the monsoon flux then tends to decrease. The recovery of the heat-low strength occurs within a few days. This is confirmed by the heat budget over the SHL area [ITD–22°N, 0–10°E] (Figure 11) computed from mesoscale simulations with MesoNH (Lafore *et al.* (1998), same set-up as in Barthe *et al.* (2009), with a uniform horizontal resolution of 20 km and twice more vertical levels below 5000 m) initiated from the ECMWF analysis at 0000 UTC and run for each individual day from 4 to 7 June. Note that the potential temperature is well correlated with the geopotential height (Lavaysse *et al.*, 2009) and is a good indicator of the heat-low. The total budget of heat and moisture for 4 June is first presented in Figure 11. As already shown by Peyrillé and Lafore (2007), the turbulent transport balances the advection for both heat and moisture. In addition, here the differentiation of horizontal and vertical advection highlights the large contribution of the horizontal advection at low levels (<1 km). The vertical advection tends to slightly moisten and cool the levels below 1 km, corresponding to a slight ascent and drying and warming (subsidence) of the levels above. The radiative term is relatively weak compared to the others and very similar from one day to the next during this period. The budget for the daytime is qualitatively similar to the 24 h budget with an increase of the tendency and turbulence terms (also a positive versus slightly negative radiative terms). In the following we present the tendency, advection and turbulence terms of heat and moisture daytime budgets for 4, 5, 6 and 7 June (Figure 11). The boundary layer warms less and moistens more during the day on 4 and 5 June due to strong advection (mainly horizontal advection) than on 6 and 7 June when the advection is reduced; the advection tends to cool and moisten the low levels as shown for the 24 h and daytime budgets. The turbulence mixes heat deeper on 5 and even more on 7 June. On 7 June, the mixing ratio is quite small so the turbulent transport even though deeper is weaker for the moisture budget.

This analysis has highlighted the existence of a heat-low induced circulation which has a negative feedback (advection of cool air) on the heat-low intensity. The solar radiation is such at this time of the year that it enables a quick restoration of the heat-low in the absence of any advection. In fact, with a daily-mean surface heat flux of 100 W m^{-2} and mean boundary-layer height of 2000 m the corresponding warming is of 4 K day^{-1} which counterbalances the cooling obtained with a mean advection (considering a mean meridional temperature gradient of 8 K over 1000 km and mean meridional wind of 6 m s^{-1}). Such a hypothesis could be investigated in further studies by using idealized simulations such as the configuration proposed by Peyrillé *et al.* (2007).

The variability of the pressure (Figure 10) and moisture (Djougou and Tamale, figure 2) in the low latitudes is weak. Thus, the variability of ΔP is dominated by the northern fluctuations. It therefore points to a predominantly continental nature of this phenomenon and highlights the major role played by the heat-low. This mechanism is controlled by the variability of the temperature, which in turn induces fluctuations of the moisture via advection. This surge mechanism and the presence of well-defined surges during the pre-onset is broadly consistent with Sultan and Janicot (2003) who highlighted the role of the heat-low in controlling the

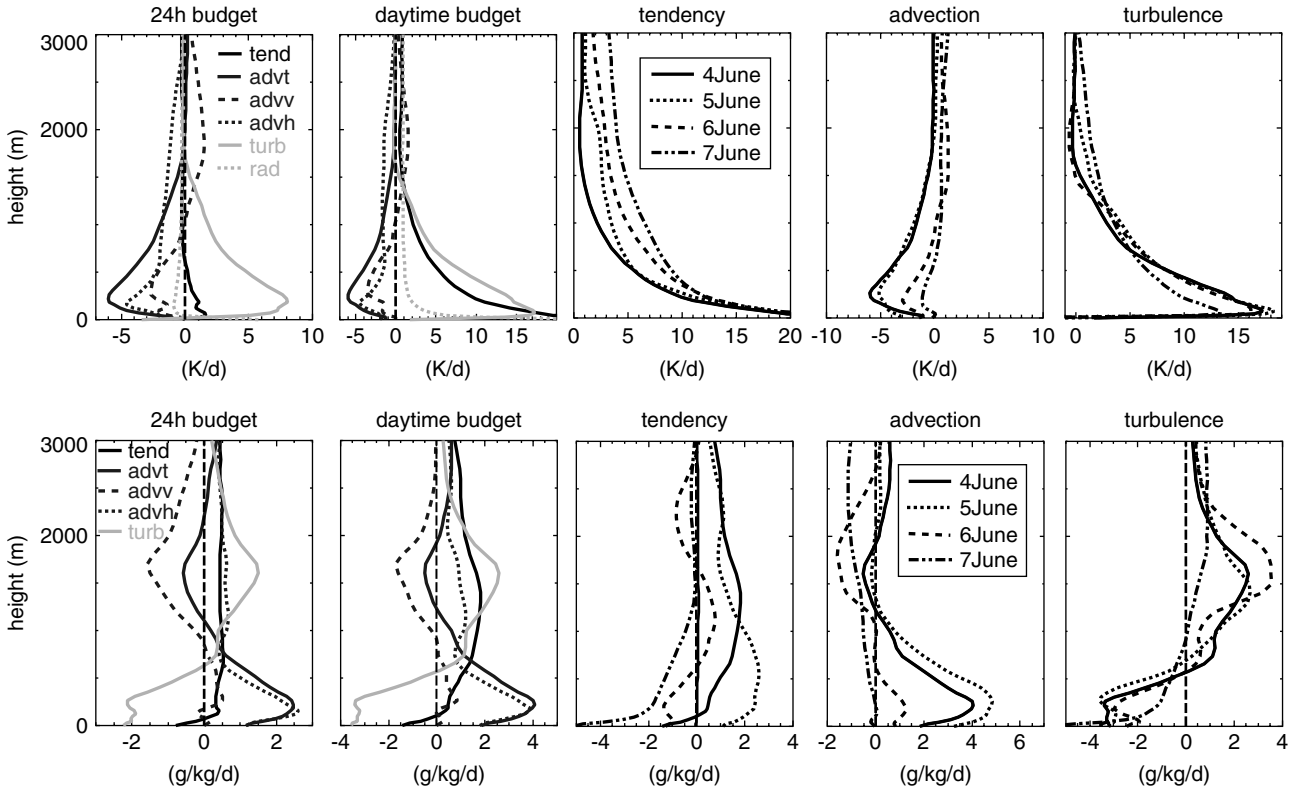

Figure 11. Heat (upper panels) and moisture (lower panels) budget over the heat-low. From left to right: the 24 h budget, the daytime budget for 4 June, then other panels corresponding to the daytime budget for 4, 5, 6 and 7 June for the tendency terms, the advection terms and the turbulence terms.

circulation in the low and mid-levels during the period preceding the monsoon onset; it operates however at a distinct, smaller time-scale.

3.2. The 7–10 June case, a propagative surge

The first case-study led to a conceptual model. Through this second case, complicated by the presence of an AEW, we highlight the differences due to the interaction with theAEW.

3.2.1. Synoptic conditions

This period follows the preceding one. The upper-level trough is still present over the area and is stationary from 7 to 10 June. An organised convective system is initiated during 8 June in the afternoon (around 1500 UTC). It was aligned southwest–northeast, from 0°E, 10°N to 8E, 20°N and passed over Niamey.

3.2.2. Existence of AEW

The existence of an AEW is highlighted by a large anomaly of the meridional wind (Figure 5). This anomaly (noted P in Figure 5) starts late 7 June at 20°E in relation with the development of daytime convection, and travels across all West Africa. Horizontal maps of positive vorticity at 850 hPa indicate the AEW's existence, propagating with a phase velocity of about 7.5 m s^{-1} (not shown). Diagnostics of Berry *et al.* (2007) reveal that this period is characterized by an enhancement of AEW activity. Horizontal wind profiles from UHF radar wind profiler observations indicate a trough in the afternoon of 8 June evidenced by a shift from northerly wind to southerly wind at 4 km height (Figure 9); note also that the AEJ is particularly strong during 8 and 9 June, located at about 12°N. Time evolution of observed winds, relative humidity and potential temperature anomaly over this period shows the characteristic structure of a wave with a southerly wind from 8 June to 9 June up to an altitude of 10 km, cooler air and moister air up to 5 km during this period (not shown), consistent with Reed *et al.* (1977). The modification of the atmosphere involves a much thicker layer for this case than the previous one. The wave is also evident in the meridional wind at 850 hPa with two vortices revealed by the streamline function (not shown).

3.2.3. Surge characteristics

Figure 8 indicates a similar evolution with a northward excursion of the ITD, although to a lesser extent, a deepening of the monsoon layer and an increase of the IWV with larger values (Figure 3 indicates that for this case the low levels are not the only contributors to the IWV variability: the AEJ layer also contributes to this variability). The maximum of temperature gradient and the minimum of pressure are also recorded just before the surge, respectively 7 June 1800 UTC and 8 June 0600 UTC, rapidly followed by an increase of the meridional wind. Figure 10 also shows a similar sequence for this surge as for the stationary one with an increase

of the pressure gradient (even though with a weaker intensity, mainly due to the contribution of northern latitudes) followed by an increase of the meridional wind and then by the increase of IWV. Therefore, the same conceptual model seems to also hold for this case. However, the AEW interacts with the heat-low and favours the coexistence of two heat-low cells present from 8 June moving westward (Figure 7). The distance between these two cells is about 2200 km, consistent with the typical length-scale of an AEW and propagates at a similar speed to that of an AEW. This was not the case for the previous surge. The two low-pressure cells induce an acceleration of the monsoon flux to their southeast flank (Figure 7). The pressure perturbation propagates westward as opposed to the previous case where it stays stationary. So, this time the pressure perturbations are partly controlled by the AEW. The westward propagation also affects the IWV: a lag is noted in Figure 2 between the maximum of the IWV occurring earlier in Gao (Niamey) than in Tombouctou (Ouagadougou).

This case thus highlights strong interactions between monsoon surge and AEW prior to the onset. After the onset, other types of interactions occur between moisture surges and AEW as shown by Barthe *et al.* (2009).

4. Criteria and modulating factors of surges

4.1. Criteria for surge identification

In this work we have mainly used an IWV-based criterion to identify the surges, as we mainly focus on water vapour variability. The IWV has the advantage of having a weak diurnal cycle as opposed to other moisture variables (low-level relative humidity and water vapour mixing ratio). Nevertheless, those moisture variables can be used equivalently and at different vertical levels up to 3 km once the diurnal cycle has been filtered out. The ITD also exhibits such surges as shown in Figures 6 and 8. The MSLP is also well correlated with the IWV and can be used as a criterion to a lesser extent. The zonal wind is not an adequate criterion as the maximum can either occur slightly before, during or after the surge. The meridional wind is a better criterion as most of the surges are slightly preceded by a maximum in the meridional wind.

4.2. Modulating factors

Besides the picture reflected by the surge composite, there is some variability among the surges as emphasized by the two case-studies. Indeed, several factors are potentially able to modulate the characteristics of the surges. As stated before, our results point to a significant role of the heat-low dynamics and AEWs. Inspection of characteristic time-scales of MSLP, geopotential height, IWV, ΔP and temperature in ECMWF analysis fields reveals (1) a single time-scale of 5 days (in the time range from 1 to 10 days) of the MSLP averaged over 15°N to 25°N in agreement with Bounoua and Krishnamurti (1991), (2) two additional time-scales but of weaker amplitude for IWV and ΔP. The latter implies that the heat-low is not the only cause of the IWV and pressure gradient pulsations. Other processes modulate their frequency. In fact, larger-scale circulations also modulate the ΔP and the IWV. Flamant *et al.* (2009) indicate the role of the upper trough in driving the monsoon surge, suggesting that upper levels might also influence the surges. Even though they are not the main driver of the ΔP, pressure fluctuations at 8–12°N induce slight modulation of the gradient. The strength of the Libyan anticyclone by controlling the Harmattan speed might modulate the recovery of the surge as strong Harmattan winds can accelerate the drying of the area. Eventually, the aerosol content, via aerosol radiative properties, modifies the characteristics of the heat budget over the heat-low and therefore can also modulate the surge characteristics. Conversely, the surges might impact the dust loads by increased surface winds. Engelstaedter and Washington (2007) suggested that the dust emission was highest over the Sahel during the monsoon onset. The topography, especially the Hoggar, is another factor that impacts the circulation and might play a role in the location of the monsoon surge, favouring a surge at the southwest of the mountains.

Variability of moist convection and cloud cover south of the ITD might also interact with these fluctuations. Deep convection north of 13°N predominantly occurs simultaneously with monsoon surges as shown for the two case-studies, suggesting a control of deep convection by the moisture increases. Nevertheless, the convection especially the organised convective systems also modulates the surges; this is suggested by wider, more abrupt, complex surges and with larger northward extension during the monsoon season (not shown).

5. Conclusion

Using ECMWF analyses and AMMA observations, we have highlighted a synoptic time-scale mode of variability of atmospheric moisture especially pronounced during the phase preceding the monsoon onset. The low levels contribute the most to this variability, which is characterized by successive northward excursions, 'surges', of the monsoon flux. The water vapour surges have a characteristic time-scale of 3–5 days and a horizontal length-scale of 1000 km. They are evident in the IWV and the ITD fluctuations. They result from an intensification of the monsoon flux through both greater amplitude and a deepening of this flow. This intensification of the monsoon flux arises from an increase of the pressure gradient controlled mainly by the northern latitudes. This points to a predominantly continental nature of this phenomenon prior to the monsoon onset. The cooling resulting from the increased monsoon flux in turn destroys the heat-low. In this phase, a partitioning of the heat-low often occurs. The intensity of the solar radiation and dry convection is such at this time of the year that they can explain the restoration of the heat-low. In this study, we have highlighted two types of surges: (1) stationary surges for

which the heat-low is the main driver and (2) propagative ones resulting from more complex interactions with African easterly waves. However, the same conceptual model holds for both. Another important conclusion is the fact that most of the variability of the IWV is carried out by the low levels (up to 3 km, Figure 3). Higher layers (from 3 to 5 km) seems to play a role in the variability of the IWV in some propagative cases.

The monsoon flux surges appear as strong fluctuations in IWV during an overall stationary period (period B in Bock *et al.*, 2008). Nevertheless they are central to the maintenance of the water vapour content during the pre-onset to onset period.

In this study, we have suggested possible relationships between the surges and convective systems. Namely, monsoon surges appear to favour deep convection. In the future, this interaction and the possible modulation of surges by convective systems could be further investigated by focusing on the monsoon season where such surges exist in the presence of frequent convective systems. These surges appear to have slightly different characteristics (less periodic, with larger latitudinal extensions).

Acknowledgements

Based on a French initiative, AMMA was built by an international scientific group and is currently funded by a large number of agencies, especially from France, UK, USA and Africa. It has been the beneficiary of a major financial contribution from the European Community's Sixth Framework Research Programme. Detailed information on scientific co-ordination and funding is available on the AMMA international website http://www.amma-international.org. The authors would like to thank M.N. Bouin, IGN, for having processed the GPS data and E. Doerflinger, CNRS, and national meteorological services from the different countries hosting GPS receivers, for having participated to the installation and maintenance of the AMMA GPS network. The lead author also thanks F. Favot for assistance on Ferret. The authors thank the anonymous reviewers whose comments greatly improved the paper.

References

Barthe C, Asencio N, Lafore J-P, Chong M, Campistron B. 2009. Multi-scale analysis of the 25–27 July 2006 convective period over Niamey: Comparison between Doppler radar observations and cloud-resolving simulations. *Q. J. R. Meteorol. Soc.* **136**(s1): 191–209.

Berry G, Thorncroft CD, Hewson T. 2007. African easterly waves during 2004: Analysis using objective techniques. *Mon. Weather Rev.* **135**: 1251–1267.

Bock O, Bouin MN, Doerflinger E, Collard P, Masson F, Meynadier R, Nahmani S, Koité M, Gaptia Lawan Balawan K, Didé F, Ouedraogo D, Pokperlaar S, Ngamini J-B, Lafore J-P, Janicot S, Guichard F, Nuret M. 2008. West African monsoon observed with ground-based GPS receivers during African Monsoon Multidisciplinary Analysis (AMMA). *J. Geophys. Res.* **113**: D21105, DOI:10.1029/2008JD010327

Bounoua L, Krishnamurti TN. 1991. Thermodynamic budget of the five day wave over the Saharan desert during summer. *Meteorol. Atmos. Phys.* **47**: 1–25.

Cadet DL, Houston SH. 1984. Precipitable water over Africa and the eastern central Atlantic Ocean during the 1979 summer. *J. Meteorol. Soc. Jpn* **62**: 761–773.

Cadet DL, Nnoli NO. 1987. Water vapour transport over Africa and the Atlantic Ocean during summer 1979. *Q. J. R. Meteorol. Soc.* **113**: 581–602.

Diedhiou A, Janicot S, Viltard A, de Felice P, Laurent H. 1999. Easterly wave regimes and associated convection over West Africa and tropical Atlantic: Results from the NCEP/NCAR and ECMWF reanalyses. *Clim. Dyn.* **15**: 795–822.

Duvel J-P. 1990. Convection over tropical Africa and the Atlantic Ocean during northern summer. Part II: Modulation by easterly waves. *Mon. Weather Rev.* **118**: 1855–1868.

Eltahir EAB, Gong C. 1996. Dynamics of wet and dry years in West Africa. *J. Climate* **9**: 1030–1042.

Engelstaedter S, Washington R. 2007. Atmospheric controls on the annual cycle of North African dust. *J. Geophys. Res.* **112**: D03103, DOI:10.1029/2006JD007195

Flamant C, Chaboureau J-P, Parker DJ, Taylor CM, Cammas J-P, Bock O, Timouk F, Pelon J. 2007. Airborne observations of the impact of a convective system on the planetary boundary layer thermodynamics and aerosol distribution in the inter-tropical discontinuity region of the West African monsoon. *Q. J. R. Meteorol. Soc.* **133**: 1175–1189.

Flamant C, Knippertz P, Parker DJ, Chaboureau J-P, Lavaysse C, Agusti-Panareda A, Kergoat L. 2009. The impact of a mesoscale convective system cold-pool on the northward propagation of the intertropical discontinuity over West Africa. *Q. J. R. Meteorol. Soc.* **135**: 139–159.

Hagos SM, Cook KH. 2007. Dynamics of the West African monsoon jump. *J. Climate* **20**: 5264–5284.

Huffman GJ, Adler RF, Bolvin DT, Gu G, Nelkin EJ, Bowman KP, Hong Y, Stocker EF, Wolff DB. 2007. The TRMM Multisatellite Precipitation Analysis (TMPA): Quasi-global, multiyear, combined-sensor precipitation estimates at fine scales. *J. Hydrometeorol.* **8**: 38–55.

Janicot S, Thorncroft CD, Ali A, Asencio N, Berry G, Bock O, Bourles B, Caniaux G, Chauvin F, Deme A, Kergoat L, Lafore J-P, Lavaysse C, Lebel T, Marticorena B, Mounier F, Nedelec P, Redelsperger J-L, Ravegnani F, Reeves CE, Roca R, de Rosnay P, Schlager H, Sultan B, Tomasini M, Ulanovsky A, ACMAD forecasters team. 2008. Large-scale overview of the summer monsoon over West Africa during the AMMA field experiment in 2006. *Ann. Geophys.* **26**: 2569–2595.

Kalapureddy M, Campistron B, Lohou F, Lothon M, Saïd F. 2009. Wind profiler observations of seasonal variability of tropospheric dynamics over West Africa. *Q. J. R. Meteorol. Soc.* **136**(s1): 77–91.

Kiladis GN, Thorncroft CD, Hall NMJ. 2006. Three-dimensional structure and dynamics of African easterly waves. Part I: Observations. *J. Atmos. Sci.* **63**: 2212–2230.

Lafore J-P, Stein J, Asencio N, Bougeault P, Ducrocq V, Duron J, Fischer C, Héreil P, Mascart P, Masson V, Pinty JP, Redelsperger J-L, Richard E, Vilà-Guerau de Arellano J. 1998. The Meso-NH Atmospheric Simulation System. Part I: Adiabatic formulation and control simulations. *Ann. Geophys.* **16**: 90–109.

Lavaysse C, Flamant C, Janicot S, Parker DJ, Lafore J-P, Sultan B, Pelon J. 2009. Seasonal evolution of the West African heat low: A climatological perspective. *Clim. Dyn.* **33**: 313–330.

Lothon M, Saïd F, Lohou F, Campistron B. 2008. Observation of the diurnal cycle in the low troposphere of West Africa. *Mon. Weather Rev.* **136**: 3477–3500.

Mekonnen A, Thorncroft CD, Aiyyer AR. 2006. Analysis of convection and its association with African easterly waves. *J. Climate* **19**: 5405–5421.

Mounier F, Kiladis GN, Janicot S. 2007. Analysis of the dominant mode of convectively coupled Kelvin waves in the West African monsoon. *J. Climate* **20**: 1487–1503.

Nuret M, Lafore J-P, Bock O, Guichard F, Agusti-Panareda A, N'Gamini J-B, Redelsperger J-L. 2008. Correction of humidity bias for Vaisala RS80-A sondes during AMMA 2006 observing period. *J. Atmos. Oceanic Technol.* **25**: 2152–2158.

Parker DJ, Burton RR, Diongue-Niang A, Ellis RJ, Felton M, Taylor CM, Thorncroft CD, Bessemoulin P, Tompkins AM. 2005. The diurnal cycle of the West African monsoon circulation. *Q. J. R. Meteorol. Soc.* **131**: 2839–2860.

Peyrillé P, Lafore J-P. 2007. An idealized two-dimensional framework to study the West African monsoon. Part II: Large-scale advection and the diurnal cycle. *J. Atmos. Sci.* **64**: 2783–2803.

Peyrillé P, Lafore J-P, Redelsperger J-L. 2007. An idealized two-dimensional framework to study the West African monsoon. Part I: Validation and key controlling factors. *J. Atmos. Sci.* **64**: 2765–2782.
Pytharoulis I, Thorncroft CD. 1999. The low-level structure of African easterly waves in 1995. *Mon. Weather Rev.* **127**: 2266–2280.
Ramel R, Gallée H, Messager C. 2006. On the northward shift of the West African monsoon. *Clim. Dyn.* **26**: 429–440.
Redelsperger J-L, Diongue A, Diedhiou A, Ceron J-P, Diop M, Gueremy J-F, Lafore J-P. 2002. Multi-scale description of a Sahelian synoptic weather system representative of the West African monsoon. *Q. J. R. Meteorol. Soc.* **128**: 1229–1257.
Redelsperger J-L, Thorncroft CD, Diedhiou A, Lebel T, Parker DJ, Polcher J. 2006. African Monsoon Multidisciplinary Analysis: An international research project and field campaign. *Bull. Am. Meteorol. Soc.* **87**: 1739–1746.
Reed RJ, Norquist DC, Recker EE. 1977. The structures and properties of African wave disturbances as observed during Phase III of GATE. *Mon. Weather Rev.* **105**: 317–333.
Smith EA. 1986. The structure of the Arabian heat low. Part I: Surface energy budget. *Mon. Weather Rev.* **114**: 1067–1083.
Sultan B, Janicot S. 2003. The West African monsoon dynamics. Part II: The 'preonset' and 'onset' of the summer monsoon. *J. Climate* **16**: 3407–3427.
Taylor CM, Parker DJ, Lloyd CR, Thorncroft CD. 2005. Observations of synoptic-scale land surface variability and its coupling with the atmosphere. *Q. J. R. Meteorol. Soc.* **131**: 913–937.
Thorncroft CD, Parker DJ, Burton RR, Diop M, Ayers JH, Barjat H, Devereau S, Diongue A, Dumelow R, Kindred DR, Price NM, Saloum M, Taylor CM, Tompkins AM. 2003. The JET2000 project: Aircraft observations of the African easterly jet and African easterly waves. *Bull. Am. Meteorol. Soc.* **84**: 337–351.
Thorncroft CD, Lafore J-P, Berry G, Roca R, Guichard F, Tomasini M, Asencio N. 2007. 'Overview of African weather systems during the summer 2006'. *CLIVAR Exchanges* **12**: 18–20.
Wheeler M, Kiladis GN. 1999. Convectively coupled equatorial waves: Analysis of clouds and temperature in the wavenumber-frequency domain. *J. Atmos. Sci.* **56**: 374–399.

